Matter

Article

# Flexibility of oxygen sublattice and hydrogen bond length predict proton mobility in ternary metal oxides

## Graphical abstract

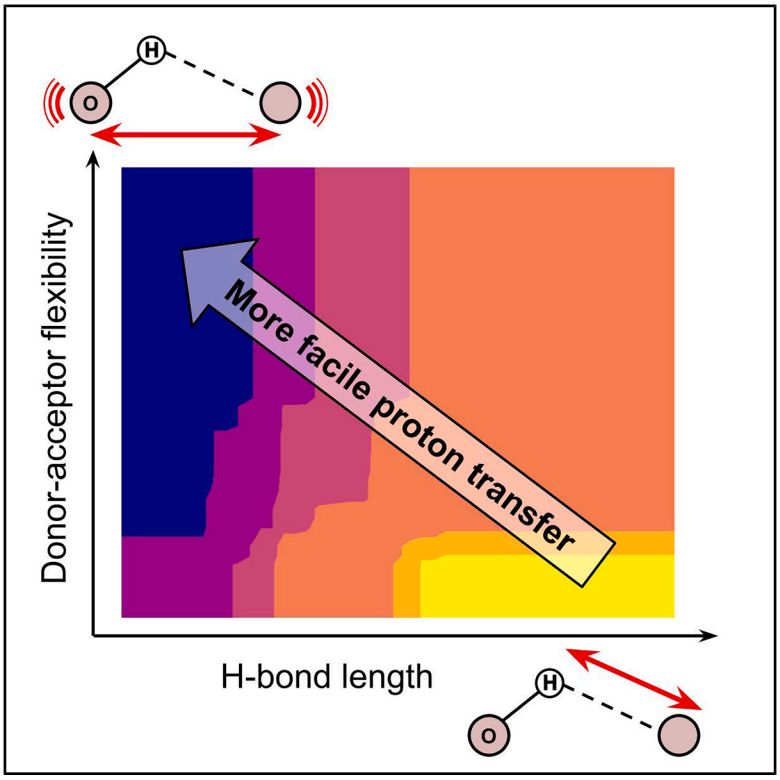


## Highlights

- Dynamic descriptor—thermal O…O fluctuation—quantifies phonon effects on $H^+$ transfer
- H-bond length and thermal O…O fluctuation top descriptor ranking for ternary oxides
- Flexible donor-acceptor pairs with short H-bonds yield lower energy barriers
- Flexible donor-acceptor pairs contract upon H insertion, reducing energy barriers

## Authors

Heejung W. Chung, Pjotrs Žguns, Ju Li, Bilge Yildiz

## Correspondence

byildiz@mit.edu

## In brief

Fast proton conduction in solid-state materials is important for many clean energy technologies. The effects of lattice dynamics on proton mobility have not been quantitatively resolved to date. We introduce a phonon-based descriptor quantifying the flexibility of the oxygen sublattice, termed thermal O…O fluctuation, and then demonstrate its usefulness for understanding proton transport using a dataset of metal oxides. Our results suggest that faster proton-conducting ternary oxides should contain percolating paths of oxide ions exhibiting high flexibility and short hydrogen bonds.

3 Understanding
Dependency and conditional studies on material behavior

Chung et al., 2026, Matter 9, 102568
March 4, 2026 
https://doi.org/10.1016/j.matt.2025.102568

CellPress

Please cite this article in press as: Chung et al., Flexibility of oxygen sublattice and hydrogen bond length predict proton mobility in ternary metal oxides, Matter (2025), https://doi.org/10.1016/j.matt.2025.102568

Matter

CellPress

Article

# Flexibility of oxygen sublattice and hydrogen bond length predict proton mobility in ternary metal oxides

Heejung W. Chung,[1] Pjotrs Žguns,[1,3] Ju Li,[1,2] and Bilge Yildiz[1,2,4,*]
[1]Department of Materials Science and Engineering, Massachusetts Institute of Technology, Cambridge, MA 02139, USA
[2]Department of Nuclear Science and Engineering, Massachusetts Institute of Technology, Cambridge, MA 02139, USA
[3]Present address: Institute of Solid State Physics, University of Latvia, Kengaraga Street 8, 1063 Riga, Latvia
[4]Lead contact
*Correspondence: byildiz@mit.edu
https://doi.org/10.1016/j.matt.2025.102568

**PROGRESS AND POTENTIAL** Fast proton conducting materials are crucial enablers of clean energy conversion and storage technologies, including fuel cells, electrolyzers, batteries, gas sensors, and low-energy brain-inspired computing. The energy efficiency of these devices depends on how quickly protons can migrate through the constituent materials. Physically based descriptors can improve our understanding of proton migration mechanisms by quantifying relevant material properties. In particular, dynamic descriptors—which capture the flexibilities of a crystal lattice—remain a promising and underexplored direction for protons in inorganic metal oxides.

In this work, we formulated a dynamic descriptor, thermal O…O fluctuation, that quantifies the flexibility of the oxygen sublattice. This descriptor captures how easily donor and acceptor oxide ions can dynamically approach each other at finite temperature to facilitate proton transfer. Using a dataset of ternary metal oxides, containing a variety of chemistries and local structures, we demonstrated that hydrogen bond length and thermal O…O fluctuation combined were the strongest predictors of proton mobility compared to other descriptors from the literature. The quantification of oxygen sublattice flexibility also enabled further analysis, which enhanced our understanding of proton migration mechanisms.

Our proposed descriptor requires only quick calculations and can therefore be incorporated into high-throughput screenings to discover promising proton-conducting ternary oxides. The improved mechanistic understanding enabled by this dynamic descriptor can also be leveraged to tune proton mobility through external fields that can maximize this descriptor.

## SUMMARY

Discovery of fast proton conductors is important for advancing clean energy technologies. This requires a better understanding of proton migration mechanisms. While structural and chemical traits of ternary metal oxides have been related to proton migration barriers, lattice dynamical effects have not been resolved quantitatively. In this work, we introduce a phonon-based dynamic descriptor, termed "thermal O…O fluctuation," quantifying the flexibility of donor-acceptor oxide-ion pairs. This enables direct comparison of O-sublattice flexibility across diverse metal oxides. Using regression models, we ranked physical descriptors as predictors of proton mobility, finding that H-bond length and thermal O…O fluctuation were the strongest descriptors. Further analysis revealed a critical O…O spacing of 2.4 Å at the transition state, which is easier to reach by more flexible donor-acceptor pairs, enabling facile proton transfer. Our results demonstrate oxygen sublattice flexibility as a dynamic descriptor and provide guiding principles for enhancing proton mobility in ternary metal oxides.

  

Please cite this article in press as: Chung et al., Flexibility of oxygen sublattice and hydrogen bond length predict proton mobility in ternary metal oxides, Matter (2025), https://doi.org/10.1016/j.matt.2025.102568



## INTRODUCTION

Inorganic proton conductors are important for a range of technologies, including protonic fuel cells and electrolyzers,[1,2] gas sensors,[3] and low-power electronics.[4] Compared to other charge carriers, protons have the advantage of being light and abundant. However, proton conductivity must be further increased to enable these technologies to become more energy-efficient and economically viable.

The class of ternary metal oxides contains many promising protonic electrolyte compositions for the temperature range of 400°C–600°C, such as Y-doped $BaZrO_3$,[5–8] as well as mixed electronic and protonic conductors, such as $SrCoO_{2.5}$[9] and $BaFeO_3$.[10] These materials, with the general compound formula of $A_xB_yO_z$ (e.g., A = Ba, Sr and B = Zr, Ce, Ti), can exhibit a wide range of symmetries and B-site coordinations. The most in-depth studies of proton-conduction mechanisms have been on perovskites[10–13] and related structures such as brownmillerites[9,14] ($ABO_{2.5}$).

In ternary metal oxides, an incorporated proton stays localized within the valence shell of a host oxide ion to form a covalently bonded hydroxyl group[15] (O-H). The proton often minimizes the energy further through a hydrogen bond (H-bond, also denoted as O-H…O), a directional interaction where the proton is electrostatically attracted to a nearby oxide ion. This hydrogen bond is essential to enable proton migration according to the two-step Grotthuss mechanism[16] (Figure 1), consisting of proton transfer from a donor to an acceptor oxide ion, followed by hydroxyl-group rotation. The second step prevents backward shuttling to the original donor and leaves the hydroxyl bond intact. The first step, widely considered to be rate-limiting in ternary oxides,[17–19] involves removing the proton from the donor's valence shell and forming a new hydroxyl group with the acceptor. For very short donor-acceptor (O…O) spacings at around 2.4 Å, the proton is embedded into the valence shells of both oxide ions, in some cases forming a nearly symmetric O-H-O bond.[15]

High-throughput studies of ternary oxides[19] have identified structural descriptors, such as H-bond length, which correlate with energy barriers. Electrostatic descriptors, including B-site cation radii and oxidation states, have also been viable descriptors for perovskites.[17] However, energy barriers showed wide variance with these structural and electrostatic descriptors alone, especially across different crystal structures.[19] Quantifying dynamic effects on proton transport presents an underdeveloped but promising direction. Earlier studies have identified phononic descriptors, for example in lithium-[20–22] and oxide-ion conducting[23] systems. In solid acids, our recent work has shown that a descriptor of lattice dynamics—specifically the phonon band center of the framework cation sublattice—correlated with the rotational flexibility of polyanion groups, which is key to the second step in the Grotthus mechanism in this class of materials.[24]

Although ternary oxides exhibit different proton-migration pathways from solid acids, case studies of perovskites have suggested the importance of lattice flexibility in facilitating proton transport. For example, first-principles calculations in $BaBO_3$ (B = Ti, Zr, Ce) showed a sharp increase in proton-transfer energy barrier with widening O…O spacing that was imposed using isotropic strain[25] (and not obtained dynamically). In addition, nudged-elastic-band simulations in O-deficient $BaFeO_3$[10] showed that donor-acceptor spacings reached 2.4 Å at the transition state, remaining consistent even with B-site dopants of varying radii[11]; energy barriers of proton transfer correlated strongly with the decrease in O…O spacing required to reach this critical transition-state spacing along the minimum-energy pathway[10,11] (discussed more in the "donor-acceptor dynamics" section). Although these results highlight the dramatic effect of donor-acceptor spacing on proton transfer, they do not quantify how phononic properties could affect the donor-acceptor spacings dynamically, the corresponding oxygen sublattice flexibility, nor its effect on the proton migration. Other case studies using molecular dynamics have observed that some phonon modes—such as O-Ce-O bending in $BaCeO_3$[26] or $ZrO_6$ octahedral tilting in Y-doped $BaZrO_3$[6]—can open up or close off proton-migration pathways. Experimentally, lattice contraction in Y-doped $BaBO_3$ (B = Zr, Ce) was shown to increase energy barriers of proton transfer, attributed to stiffer B-O stretching.[27,28] Notably, these works directly linked proton transport to specific phonon modes. However, no phonon-based descriptors were proposed or quantified, and each study focused on a narrow range of perovskites and phonon modes. A few early studies of perovskites did find correlations between proton-transfer barriers and tabulated descriptors—such as average atomic mass—used as proxies for phonon frequencies.[29] However, we expect the key phonon modes affecting proton transfer to change for materials other than perovskites, making these simple descriptors insufficient for analysis across different crystal structures. A broader comparison across varying chemistries and structures is required to strengthen our understanding of how lattice flexibility affects proton mobility and guide the design of improved proton-conducting oxides. There remains a clear gap and the need to quantify lattice flexibility through a generalized phonon-based descriptor.

In the present study, we formulated a generalized, quantitative measure of donor-acceptor flexibility called thermal O…O fluctuation and then assessed its importance relative to other

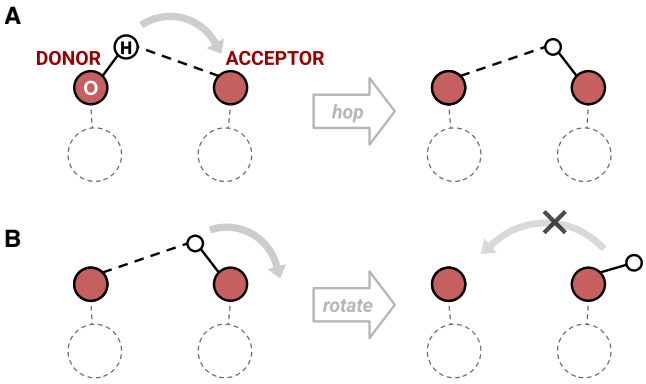


**Figure 1. Two-step Grotthuss mechanism of proton transport**

(A) Proton-transfer step where proton transfers from a donor oxide ion to an acceptor oxide ion across a hydrogen bond.

(B) Lattice-rearranging step where proton is brought away from the original donor by rotation of the hydroxyl group to prevent back-and-forth shuttling. Dashed circles represent local environments surrounding a donor-acceptor pair, since these can vary across different crystal structures.

Please cite this article in press as: Chung et al., Flexibility of oxygen sublattice and hydrogen bond length predict proton mobility in ternary metal oxides, Matter (2025), https://doi.org/10.1016/j.matt.2025.102568



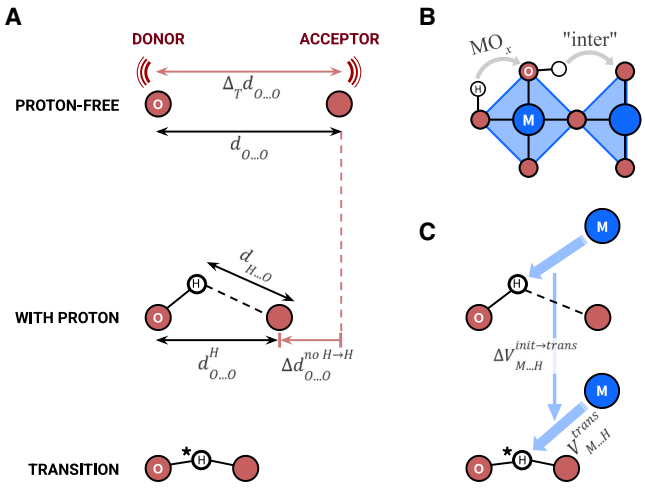


**Figure 2. Configurations and descriptors for proton transfer across a single donor-acceptor pair**

(A) Geometric descriptors marked in black, including donor-acceptor spacings in the proton-free $d_{O\ldots O}$ and protonated $d^{H}_{O\ldots O}$ configurations, along with H-bond length $d_{H\ldots O}$; dynamic descriptors shown in red, including thermal O…O fluctuations $\Delta_T d_{O\ldots O}$ and change in O…O spacing $\Delta d^{no\ H\to H}_{O\ldots O}$ from the proton-free to the protonated configuration.

(B) Coordination of metal-oxygen polyhedron containing donor and acceptor, e.g., $MO_6$ for proton transfer across octahedron edge (undefined for inter-polyhedral jumps).

(C) Electrostatic descriptors in blue, including Coulombic repulsions from the nearest cation, M, at transition state $V^{trans}_{M\ldots H}$ and the change in this repulsion $\Delta V^{init\to trans}_{M\ldots H}$ from the protonated initial state to the transition state.

structural, electrostatic, and dynamic descriptors. We identified H-bond length and thermal O…O fluctuations as the primary descriptors that could best predict energy barriers of proton transfer, capturing key trends across a wide range of local structural and chemical environments. The resulting model suggested that donor-acceptor pairs exhibiting strong H-bonding and high flexibility would be ideal for proton transfer.

Connecting more to underlying mechanisms, we found that more flexible O…O pairs contracted more upon H-bond formation. These contractions brought the donor and acceptor closer to a critical O…O spacing of 2.4 Å at the transition state. Facile contractions enabled by O…O flexibility gave rise to lower proton-transfer energy barriers. In addition, O…O flexibility enabled migrating protons to avoid nearby cations, thereby reducing electrostatic repulsion. Finally, our approach further allows us to identify the phonon modes that dominate thermal O…O fluctuations and may facilitate proton conduction. We performed this mode extraction on a few donor-acceptor pairs, which exhibited higher proton mobility. Overall, our work demonstrates how the dynamics of the oxygen sublattice crucially helps predict proton-transfer energy barriers and presents guiding principles for optimizing proton conduction in metal oxides.

## PROPERTIES AFFECTING PROTON TRANSFER AND THEIR PHYSICAL DESCRIPTORS

Unlike other ionic species, a proton lacks its own electrons and strongly prefers to stay embedded within the valence shell of an oxide ion. Pulling a proton away from its donor and depleting it of electron density incurs a large energy cost. This shapes the proton-transfer migration pathway, and surrounding atoms adjust their positions to support this embedding.[15] Although ternary oxides present a structurally diverse set of materials, it is desirable to devise physical descriptors that underscore commonalities controlling the proton-transfer mechanism.

Physically based descriptors can capture these effects on transport mechanisms, as well as how they vary with composition and crystal structure. We define descriptors as featurization of the electronic, phononic, or atomic structure that correlate with ionic mobility through connection to the underlying transport mechanisms. The most useful descriptors are physically interpretable, generalizable, and feasible to calculate or measure. In our analysis, we consider structural, electrostatic, and dynamic descriptors of proton transfer. Since H-bond formation and proton transfer can incur significant lattice distortions, we distinguish between three configurations associated with each donor-acceptor pair within a material. These are the proton-free, protonated, and transition-state structures shown in Figure 2. Bond lengths and separation distances within these configurations could be used as geometric or structural descriptors, also as shown in Figure 2.

### Local structure and H-bonding strength

Reflecting the attraction between a proton and the valence shell of a neighboring acceptor oxide ion, H-bonding strength plays a crucial role in proton transfer. The effect is so dramatic that transfer practically cannot proceed in many oxides unless an H-bond has formed first.[15]

This property is often quantified through geometric parameters, most commonly the H-bond length. Islam et al. found clear trends between H-bond lengths and proton-transfer energy barriers after performing a high-throughput screening of ternary oxides,[19] although there was large variability across different stoichiometries and coordinations. They also found that the coordinations of metal-oxygen polyhedra ($MO_x$) correlated somewhat with energy barriers, proposing that corner-connected $MO_6$ octahedra could enable more facile proton transfer. We therefore considered metal-oxygen polyhedral coordination as one structural descriptor. For donor-acceptor pairs where the proton transferred across a polyhedral edge, we used the coordination of this polyhedron. All other donor-acceptor pairs represented inter-polyhedral proton transfer, so their cation coordination was undefined. Donor-acceptor spacings have also been shown to affect H-bond strengths and proton-transfer energy barriers. In addition to H-bond length $d_{H\ldots O}$, and cation coordination, we therefore included proton-free and protonated O…O spacings, $d_{O\ldots O}$ and $d^{H}_{O\ldots O}$, respectively, as relevant descriptors (Figures 2A and 2B).

### Electrostatic repulsion from nearest cation

Nearby cations can impede transport by affecting H-bonding geometries or, more directly, by electrostatically repelling a proton at the transition state.[15] In a high-throughput study of perovskites,[17] Islam et al. correlated energy barrier with B-site cation radius, oxidation state, and proton-cation distance. Using these descriptors, they showed how a larger B-site cation could push a

proton away from the donor-acceptor axis, increasing H-bond length and forcing the proton into regions with depleted electron density. However, these descriptors were not shown to correlate with energy barriers in their subsequent study of broader ternary oxides,[19] likely because of varying H-bonding geometries across different crystal structures.

We quantified these effects using the Coulomb repulsion:

$$V^{trans}_{M\ldots H} = k_e \frac{z_M \cdot e^2}{d^{trans}_{M\ldots H}}$$

where $d^{trans}_{M\ldots H}$ is the distance between the proton and nearest cation at the transition state (Figure 2C), $z_M$ is the nearest cation's oxidation state, $e$ is the charge of an electron, and $k_e$ is Coulomb's constant. To capture contribution to energy barriers, we also included the change in repulsion energy $\Delta V^{init\rightarrow trans}_{M\ldots H} = V^{trans}_{M\ldots H} - V^{H}_{M\ldots H}$ from the protonated initial state to the transition state.

### Donor-acceptor dynamics

Unlike the broadly studied H-bonding effects, lattice dynamical effects on proton transport have been limited to a few case studies of perovskite oxides.[6,10,11,25,29,30] Using ab initio molecular dynamics in $BaCeO_3$, Kreuer et al. observed proton transfer only if, first, the O-Ce-O bending mode dynamically reduced donor-acceptor spacing and enabled H-bond formation.[26] Recently, the nudged-elastic-band method was used to investigate proton transport within O-deficient[10] and doped[11] $BaFeO_{3-\delta}$, where all donor-acceptor pairs reached a transition-state spacing near 2.4 Å. Using the minimum-energy pathways from energy-barrier calculations, they took the change from the initial O…O spacing to 2.4 Å—the critical transition-state spacing—as their dynamic descriptor. They found that proton transfer was more difficult across O…O pairs that underwent more compression along the minimum-energy pathway. This suggested that the lattice distortion required to reach the critical spacing of 2.4 Å contributes significantly to proton-transfer energy barriers. Extrapolating to other materials, we would expect to observe lower energy penalties in lattices that can accommodate these compressions more easily.

In order to quantify O-sublattice flexibility, we used two descriptors (Figure 2A). We sought to quantify donor-acceptor flexibility as an intrinsic material property that we could extract from the phonon band structure of the proton-free compounds. To this end, we formulated a descriptor called thermal O…O fluctuation, $\Delta_T d_{O\ \ldots\ O}$, shown in Figure 2A, which estimates the variance in spacing between donor-acceptor pairs at a given temperature. Quantification of this descriptor can enable generalized comparison across diverse chemistries and structures of ternary oxides. In the next sections, we will introduce this dynamic descriptor in detail, then demonstrate its strength in predicting proton transfer barriers, as well as its connection to H-bonding and proton-transfer mechanisms.

In addition, we have quantified the change in O…O spacing from the proton-free to the protonated state (Figure 2A). If H-bond formation induces more of this contraction $\Delta d^{no\ H\rightarrow H}_{O\ldots O} = d^{H}_{O\ldots O} - d^{no\ H}_{O\ldots O}$, then the structure requires less further deformation to reach the critical O…O spacing of 2.4 Å during proton migration. While seemingly this is a geometric quantity, the extent of contraction of the O…O spacing upon protonation depends on the flexibility of the lattice, which is a dynamic characteristic. A summary of all physical descriptors we considered can be found in Table 1.

## QUANTIFYING THERMAL O…O FLUCTUATIONS

### Formulation

We aimed to capture the flexibility of the oxygen sublattice as a function of a material's phonon band structure. Adapted from the thermal displacements[31] of atoms, thermal O…O fluctuation provides an estimate of the variance in spacing between two oxide-ion sites, $j$ and $k$, at finite temperature $T$:

$$(\Delta_T d_{O\ldots O})^2 = \frac{1}{M_{\mathbf{q}}} \sum_{\lambda,\boldsymbol{q}}^{M_{\mathbf{q}}\times 3N} \frac{A(\omega_{\lambda,\boldsymbol{q}}, T)}{m} \epsilon_{j,k,\lambda,\boldsymbol{q}}\,, \qquad \text{(Equation 1)}$$

where the primitive cell contains $N$ sites, and $m$ is the mass of the oxide ion. Each term in the summation captures the fluctuation in O…O spacing induced by a single mode, indexed by the q-point $\boldsymbol{q}$ and band $\lambda$. These contributions are aggregated over a total of $3N$ bands across the Brillouin zone with $M_{\boldsymbol{q}}$ sampled q-points. The amplitude of each mode

$$A(\omega_{\lambda,\boldsymbol{q}}, T) = \frac{\hbar}{\omega_{\lambda,\boldsymbol{q}}} \left( \frac{1}{2} + n_{\text{pop}}(\omega_{\lambda,\boldsymbol{q}}, T) \right)$$

includes phonon population $n_{\text{pop}}(\omega_{\lambda,\boldsymbol{q}}, T) = \left[\exp\left(\hbar\omega_{\lambda,\boldsymbol{q}} T/k_B\right) - 1\right]^{-1}$ and captures dependence on frequency $\omega_{\lambda,\boldsymbol{q}}$ and temperature $T$, since lower-frequency modes require less thermal energy to activate. The contraction factor for each mode

$$\epsilon_{j,k,\lambda,q} = \left| \hat{\mathbf{r}}_{j\rightarrow k} \cdot \left( \exp(i\boldsymbol{q}\cdot\boldsymbol{x}_j)\, \hat{\boldsymbol{e}}^{(j)}_{\lambda,\boldsymbol{q}} - \exp(i\boldsymbol{q}\cdot\boldsymbol{x}_k)\, \hat{\boldsymbol{e}}^{(k)}_{\lambda,\boldsymbol{q}} \right) \right|^2$$

is calculated by projecting the $j^{th}$ and $k^{th}$ eigen displacements—calculated from eigenvectors $\hat{\boldsymbol{e}}^{(j)}_{\lambda,\boldsymbol{q}}$ and $\hat{\boldsymbol{e}}^{(k)}_{\lambda,\boldsymbol{q}}$—onto the axis $\hat{\mathbf{r}}_{j\rightarrow k}$ connecting their equilibrium positions $\boldsymbol{x}_j$ and $\boldsymbol{x}_k$. Since this is a pairwise quantity, a single material may be characterized by multiple thermal O…O fluctuations, one for each symmetrically unique O…O pair.

### Illustration of thermal O…O fluctuations and dominant phonon modes in $BaZrO_3$

We used cubic $BaZrO_3$ as a case study to observe which phonon dynamics most affect thermal O…O fluctuations, treating nearest-neighbor oxide ions as a donor-acceptor pair. Figure 3A shows a projected phonon band structure, where each point corresponds to the result of a term in the summation in Equation 1. Phonon modes inducing larger O…O fluctuations are assigned darker colors, and regions of the dispersion colored in yellow introduce negligible O…O fluctuations. The phonon modes that give rise to the largest O…O fluctuations, labeled A and B in Figure 3B, match those identified in the literature.[6,25,26,30]

Please cite this article in press as: Chung et al., Flexibility of oxygen sublattice and hydrogen bond length predict proton mobility in ternary metal oxides, Matter (2025), https://doi.org/10.1016/j.matt.2025.102568



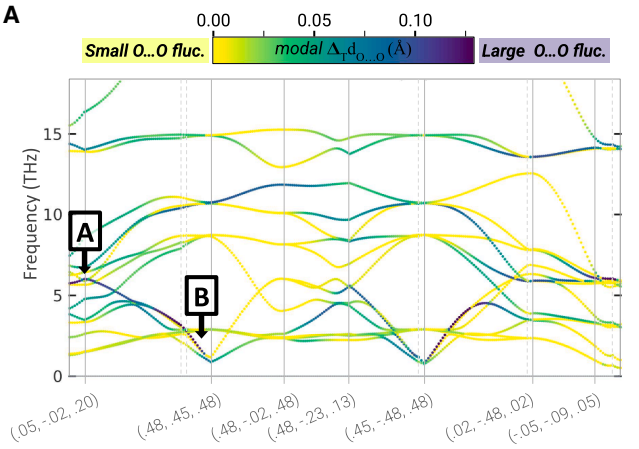


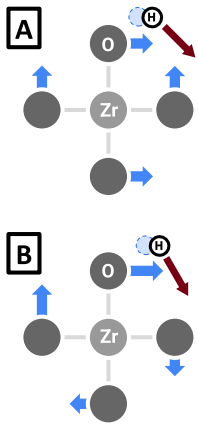


**Figure 3. Modal contributions to thermal O…O fluctuations for cubic $BaZrO_3$**

(A) Projected phonon band structure calculated, where modes shown by darker colors are predicted to induce larger fluctuations in O…O spacing as computed at 600 K.

(B) Phonon modes that induce larger fluctuations in O…O spacing include O-B-O bending (mode A) and a combination of O-B-O bending with octahedral tilting (mode B).

Mode A shows the O-B-O bending mode, and Mode B is a combination of O-B-O bending with octahedral tilting.

## APPROACH TO DATA ANALYSIS

We constructed a dataset (Table 2) with the aim of investigating the relations between our proposed physical descriptors and proton-transfer barriers across different crystal structures. In particular, we performed a systematic comparison of structural, electrostatic, and dynamic descriptors, using regression models trained to predict energy barrier $E_a$ of proton transfer.

**Table 1. Summary of physical descriptors of proton transfer in ternary oxides**

| | Notation | Descriptor | Configuration(s) |
|---|---|---|---|
| Structural (Å) | $d_{O...O}$ | O…O spacing | proton-free |
| | $d^{H}_{O...O}$ | O…O spacing after H-bond formation | with H |
| | $d_{H...O}$ | H-bond length | with H |
| | $MO_x$ | coordination of metal-oxygen polyhedron containing donor and acceptor | proton-free |
| Electrostatic (eV) | $V^{trans}_{M...H}$ | nearest cation-proton Coulombic repulsion | transition-state |
| | $\Delta V^{init\rightarrow trans}_{M...H}$ | change in repulsion during proton transfer | with H → transition |
| Dynamic (Å) | $\Delta_T d_{O...O}$ | thermal O…O fluctuation | proton-free |
| | $\Delta d^{no\ H\rightarrow H}_{O...O}$ | change in O…O spacing upon H-bond formation | proton-free → with H |

Notation listed for each descriptor, along with configuration(s) from which each descriptor is extracted. The configurations are shown in Figure 2.

### Dataset with energy barriers of proton transfer in ternary oxides

For our training data, we computed descriptors and energy barriers for 153 symmetrically unique O…O pairs found in 12 ternary oxides (Figures 4A–4C). Although the dataset is dominated by elements such as Mo, Mn, and W, it nevertheless spans a wide range of energy barriers, crystal symmetries, metal-oxygen coordination polyhedra, oxidation states, and local environments for proton migration. These form a notably diverse and comprehensive dataset of proton-conducting ternary oxides, enabling us to assess how well each descriptor could generalize.

In order to evaluate our regression models, discussed below, we also constructed an independent test dataset of 70 O…O pairs from six perovskites, including some whose proton conductivities have been previously studied.[12] We performed no analysis on these test data until after the final model had been chosen and trained.

### Regression model for predicting energy barriers

To quantify the relative strengths of descriptors in predicting proton-transfer energy barriers, we used the histogram-based gradient-boosted decision tree (HGBDT) regression model.[33] A decision tree is essentially a series of nested if-statements that operate on inputs to determine the predicted output—an energy barrier in this case. Energy barriers are first discretized into bins. During optimization, if-statement conditions are selected greedily, based on which will best separate these bins of energy barriers. Since individual decision trees suffer from overfitting, an ensemble is trained using gradient-boosting, which encourages trees to compensate for each other's errors. Given the modest size of our dataset, HGBDTs offer a good balance between expressivity, regularization, and interpretability. Unlike more complex deep learning models that risk overfitting, HGBDTs effectively capture nonlinear relationships while maintaining generalizability.

Another advantage of this model is the ability to test the existence or absence of monotonic relations between inputs and outputs, enabling both regularization and interpretability. For instance, we could constrain the model's predicted $E_a$ to monotonically decrease with increasing thermal O…O fluctuation. By training multiple HGBDTs under different constraints—either non-monotonic, increasing, or decreasing—we could observe which parameters led to the prediction of energy barriers with the least error.

Please cite this article in press as: Chung et al., Flexibility of oxygen sublattice and hydrogen bond length predict proton mobility in ternary metal oxides, Matter (2025), https://doi.org/10.1016/j.matt.2025.102568



**Table 2. Materials included in train and test datasets**

| Compound | MPID | Space group | O … O pairs | $E_a$ (eV) | Low-/High-$E_a$ $MO_x$ |
|---|---|---|---|---|---|
| | | Train and validation | | | |
| $MnMoO_4$ | mp-19081 | C2/m | 25 | 0.03–1.27 | $MnO_6/MoO_4$ |
| $Eu_3MoO_7$ | mp-1213342 | $P2_12_12_1$ | 33 | 0.07–0.71 | $EuO_7/EuO_7$ |
| $MoPO_5$ | mp-26572 | Pnma | 18 | 0.08–1.18 | Interpolyhedral/$PO_4$ |
| $CoWO_4$ | mp-19092 | P2/c | 13 | 0.09–1.42 | Interpolyhedral/$WO_6$ |
| $TaFeO_4$ | mp-755628 | P2/c | 15 | 0.09–1.42 | Interpolyhedral/$TaO_6$ |
| $CaMoO_3$ | mp-19012 | Pnma | 8 | 0.10–0.58 | $CaO_8/CaO_8$ |
| $Tb_2Mo_2O_7$ | mp-19200 | Fd $\bar{3}$ m | 4 | 0.11–0.57 | $TbO_8/TbO_8$ |
| $EuMnO_3$ | mp-20614 | Pnma | 9 | 0.15–0.30 | $EuO_8/EuO_8$ |
| $UMnO_4$ | mp-19173 | Imma | 11 | 0.16–0.91 | $MnO_6/MnO_6$ |
| $CrMoO_4$ | mp-1213733 | C2/m | 7 | 0.17–1.27 | inter-polyhedral/$CrO_6$ |
| $Nd_2Mo_2O_7$ | mp-33803 | Fd $\bar{3}$ m | 3 | 0.22–0.78 | $NdO_8/NdO_8$ |
| $Ni(BiO_3)_2$ | mp-1101457 | $P4_2/mnm$ | 7 | 0.25–0.99 | inter-polyhedral/$NiO_6$ |
| | | Test | | | |
| $CaZrO_3$ | mp-4571 | Pnma | 9 | 0.10–1.27 | all $BO_6$ octahedra |
| $CaMnO_3$ | mp-19201 | Pnma | 9 | 0.14–0.42 | – |
| $BaZrO_3$ | mp-3834 | Pm $\bar{3}$ m | 1 | 0.18 | – |
| $BaTiO_3$ | mp-558125 | $C222_1$ | 44 | 0.19–0.81 | – |
| $BaFeO_3$ | mp-1192651 | $P6_2/mmc$ | 6 | 0.22–0.99 | – |
| $SrNbO_3$ | mp-10339 | Pnma | 1 | 1.12 | – |

Chemical formula, Materials Project[32] identifier (MPID), space group, number of symmetrically unique O…O pairs, range of energy barriers, and $MO_x$ polyhedra with highest and lowest energy barriers, listed for each crystal structure in the training and testing datasets.

### Ranking descriptors by predictive importance

Since structural, electrostatic, and dynamic properties are interrelated, some of our proposed descriptors may correlate with one another. In order to remove redundancies and identify which descriptors mattered most for predicting energy barriers, we used the sequential feature selection (SFS) algorithm[34] (Figure 4D).

In the first step, we fitted $k = 8$ univariate models, each using a different descriptor as input to predict energy barrier, where $k$ was the total number of descriptors to rank. The descriptor yielding the lowest root-mean-squared error (RMSE) under 5-fold cross-validation (Section S1) was selected as the most important descriptor.

Following the greedy SFS algorithm, we assumed the globally optimal model would ultimately include this first descriptor among its inputs. In the second step, we therefore fitted $k$-1 bivariate regressions, where each model incorporated the top-ranked descriptor from the first step as a fixed input. The other input was selected from the remaining unranked descriptors, and the second-most important descriptor was determined based on RMSE.

The third step involved $k$-2 trivariate models, holding the two most important descriptors fixed to determine the next-most important descriptor. These iterations proceeded until all descriptors were ranked, ensuring that the most informative features were identified in a systematic manner while accounting for potential descriptor interactions.

When this method was applied to our training data, the best-performing model was an HGBDT predicting energy barriers from H-bond length and thermal O…O fluctuations (Section S2). As detailed further in the results and discussion, we observed negligible improvements in accuracy when models took more than these descriptors as input.

## RESULTS AND DISCUSSION

### H-bonding, metal-oxygen polyhedra, and oxygen lattice dynamic descriptors correlate individually with energy barrier

Univariate analysis shows that among the eight descriptors we considered, only H-bond length, metal-oxygen polyhedra, and the two dynamic descriptors appeared to correlate well with energy barrier, while other descriptors had lower Pearson correlation coefficients (Figure 5). Since these coefficients can only capture linear relationships, we also inspected scatterplots of each individual descriptor with energy barriers. The dynamic descriptors and metal-oxygen coordination were the only other descriptors that qualitatively appeared to correlate with $E_a$ (Figure 6).

Shorter H-bonds corresponded to more facile proton transfer (Figure 6A), although we observed a sudden increase in slope and variance for $d_{H\ldots O}$ exceeding 2.3 Å. This increased scatter is expected for longer H-bonds as they become less directional.[35] Indeed, H-bonds may not even form at large O…O spacings, making $d_{H\ldots O}$ a simple measure of proton-acceptor distance rather than a physically meaningful H-bond length.

Thermal O…O fluctuation $\Delta_T d_{O\ldots O}$ showed a negative correlation (Figure 6B), demonstrating that more flexible donor-acceptor pairs tended to enable more facile proton transfer. Change in O…O spacing upon H insertion $\Delta d_{O\ldots O}^{no\ H \rightarrow H}$ was positively correlated with $E_a$ (Figure 6C). In other words, lower-barrier pairs underwent more negative changes in spacing, indicating

Please cite this article in press as: Chung et al., Flexibility of oxygen sublattice and hydrogen bond length predict proton mobility in ternary metal oxides, Matter (2025), https://doi.org/10.1016/j.matt.2025.102568



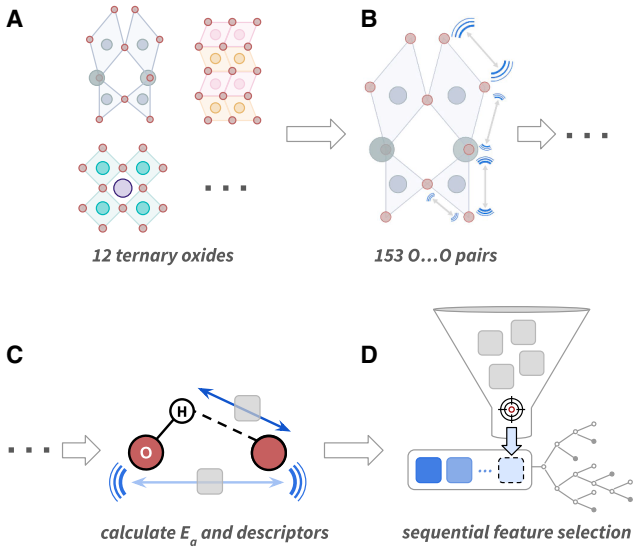


**Figure 4. Overview of approach for data collection and descriptor ranking**

(A) Set of ternary oxides expected to be stable with H insertion[19] and further screened for thermal stability.

(B) Symmetrically unique donor-acceptor pairs found within ternary oxides being studied.

(C) Descriptors and energy barriers calculated for each donor-acceptor pair using finite displacements, structural relaxations, and CI-NEB calculations.

(D) Ranking of descriptors according to their importance, based on which input yields biggest improvement in accuracy for predicting energy barrier, and selected sequentially by adding inputs to decision-tree regression model.

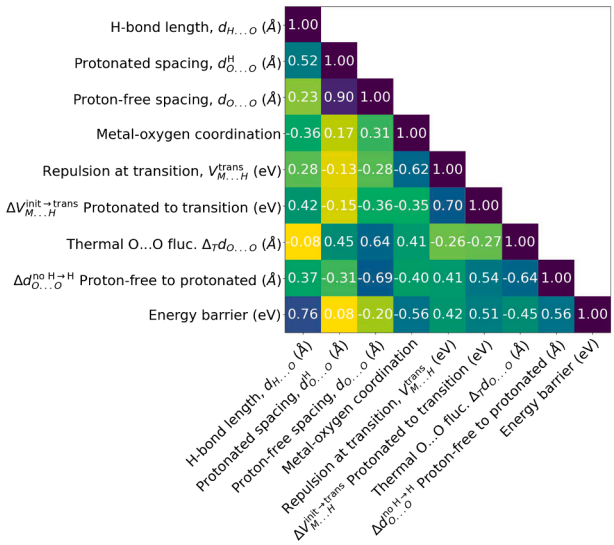


**Figure 5. Correlation matrix for all descriptors and energy barriers**

Pearson correlation coefficients between pairs of descriptors, as well as correlations of descriptors with energy barriers.

larger O…O contraction enabled by greater flexibility. We also observed that energy barriers were lower for protons migrating along edges of polyhedra with higher coordinations (Figure 6D). This may arise from electrostatic effects, as suggested by the sizable correlation between cation coordination and $V^{trans}_{M\cdots H}$ (Figure 5).

While H-bond lengths and dynamic descriptors showed clear trends with energy barriers, other descriptors exhibited weak correlations. A univariate, linear analysis cannot sufficiently quantify dependencies between descriptors and proton transfer. More expressive, multivariate modeling is essential for accurately predicting energy barriers, and our further quantitative analysis will show how O…O flexibility combines with other properties to affect proton transfer.

## Primary descriptors: H-bond length and thermal O…O fluctuation

To identify which physical descriptors most strongly relate to proton transfer, we performed the SFS algorithm, and the resulting descriptor rankings are shown on the *y*-axis in Figure 7 with model performance on the *x*-axis. From top to bottom, the plotted RMSEs correspond to model performances as more descriptors were added sequentially as inputs. H-bond length was most predictive for univariate regression of energy barriers, yielding an RMSE near 0.20 eV. The bivariate model, taking H-bond length and thermal O…O fluctuation as inputs, had a significantly lower error around 0.16 eV.

As the SFS algorithm found more descriptors (the lower ranked descriptors) sequentially, the decreases in RMSE were all within error. Therefore, we determined that the most appropriate model with a minimum set of strongest physical descriptors would be the bivariate HGBDT, with H-bond length and thermal O…O fluctuations, yielding decent accuracy without overfitting. To check that the greedy assumption of SFS held for this task, we also performed an exhaustive feature search, which obtained the exact same result in ranking the descriptors (Section S2).

## Bivariate model from primary descriptors

Here, we present our final regression model, which can estimate energy barriers from our two primary descriptors as found above. This analysis enables evaluation of their combined predictive strength and suggests principles that dictate the ease of proton transfer in ternary oxides. Our dataset is shown on a scatterplot in Figure 8A, with H-bond length on the *x*-axis and thermal O…O fluctuation on the *y*-axis. Each point corresponds to a symmetrically unique donor-acceptor pair, where the shape indicates the compound containing the oxide-ion pair; for example, all circles represent different O…O pairs found within $CaMoO_3$. The color scale denotes the energy barrier for proton transfer across the O…O pair. The pairs with the most facile proton transfer are in dark purple and those with the highest barriers are in yellow.

We found that the top two descriptors for predicting $E_a$—H-bond length and thermal O…O fluctuation—lacked correlation with each other (Figure 5), a promising indication that we were fitting a function of independent variables. The color gradient for $E_a$ observed in Figure 8A also showed qualitatively that the combination of H-bond length with thermal O…O fluctuation effectively separated low-barrier pairs from high-barrier pairs.

Please cite this article in press as: Chung et al., Flexibility of oxygen sublattice and hydrogen bond length predict proton mobility in ternary metal oxides, Matter (2025), https://doi.org/10.1016/j.matt.2025.102568



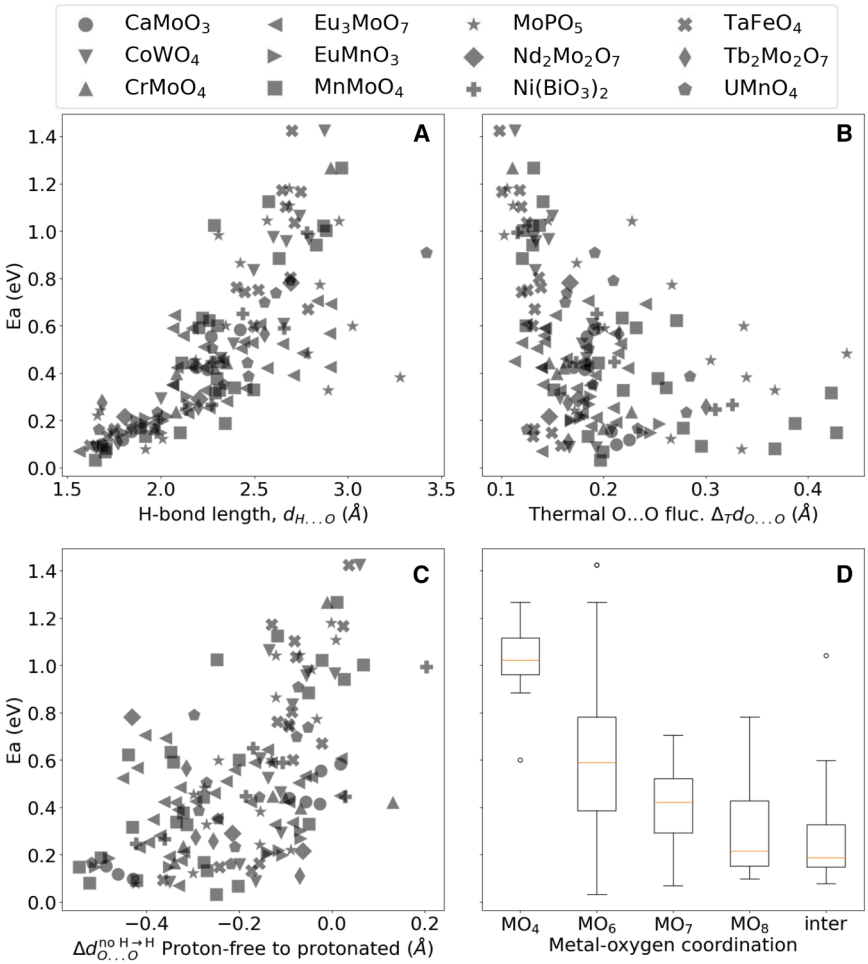


**Figure 6. Dependence of proton-transfer energy barrier on descriptors**

Points in scatterplot are symmetrically unique O…O pairs in training dataset, with shape specifying material containing O…O pair (e.g., squares for O…O pairs within $MnMoO_4$). Energy barrier plotted against (A) H-bond length, (B) thermal O…O fluctuation, (C) change in O…O spacing from proton-free to protonated state, and (D) coordination of $MO_x$ polyhedron whose edge is traversed during proton transfer.

A more quantitative analysis could be found using our HGBDT model, visualized as a heatmap of the predicted energy barrier as a function of our two descriptors (Figure 8B). A grid search of hyperparameters identified the optimal monotonic constraints as positive for H-bond length and negative for thermal O…O fluctuation. This can be seen in Figure 8B, where the color changes from yellow (high-barrier) in the bottom-right to dark purple (low-barrier) in the top-left. This model suggests some key guidelines for optimizing proton conduction; the lowest energy barriers were predicted for O…O pairs exhibiting strong H-bonding ($d_{H...O} < 2.0$ Å) and high flexibility ($\Delta_T d_{O...O} > 0.15$ Å).

Interestingly, our model appeared to establish cutoffs for H-bond length and thermal O…O fluctuations, rather than predicting gradual changes in energy barrier with either of these inputs. Thermal O…O fluctuations below 0.13 Å did not affect $E_a$ predictions nor did H-bond lengths above 2.5 Å. This cutoff is similar to the one at 2.3 Å, which we observed in our univariate analysis (Figure 6A), where the lack of H-bonding for very long $d_{H...O}$ made the descriptor less physically meaningful.

Overall, our model achieved a 5-fold cross-validated RMSE of 0.16 eV and an $R^2$ value of 0.75 for the training set. We then applied the same model to the test set, yielding an RMSE of 0.17 eV and an $R^2$ value of 0.51. One test outlier, $SrNbO_3$, heavily skewed the $R^2$ score, which was 0.64 for the remaining test data (Section S3). Although unbiased measures

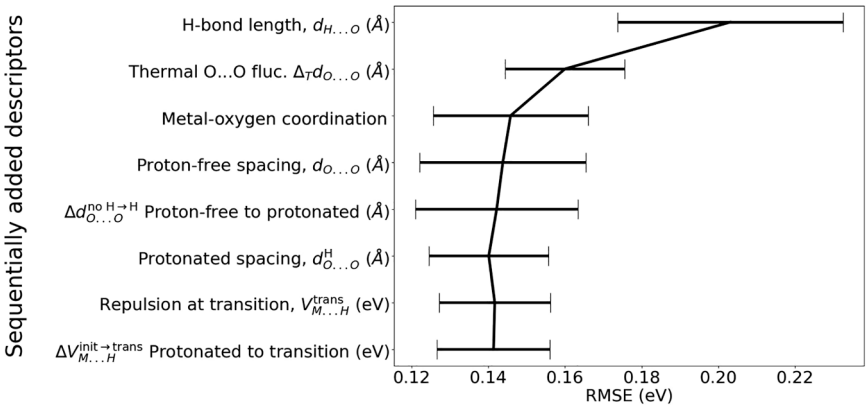


**Figure 7. Rankings of physical descriptors found by sequential feature selection**

Descriptors listed in order from most to least predictive of proton-transfer energy barriers, with importance evaluated based on largest decrease in error. From top to bottom, RMSE plotted for increasing number of inputs, with univariate model taking $d_{H...O}$ as input, then bivariate ($d_{H...O}$ and $\Delta_T d_{O...O}$), then trivariate ($d_{H...O}$, $\Delta_T d_{O...O}$, and metal-oxygen coordination), and so on.

Please cite this article in press as: Chung et al., Flexibility of oxygen sublattice and hydrogen bond length predict proton mobility in ternary metal oxides, Matter (2025), https://doi.org/10.1016/j.matt.2025.102568



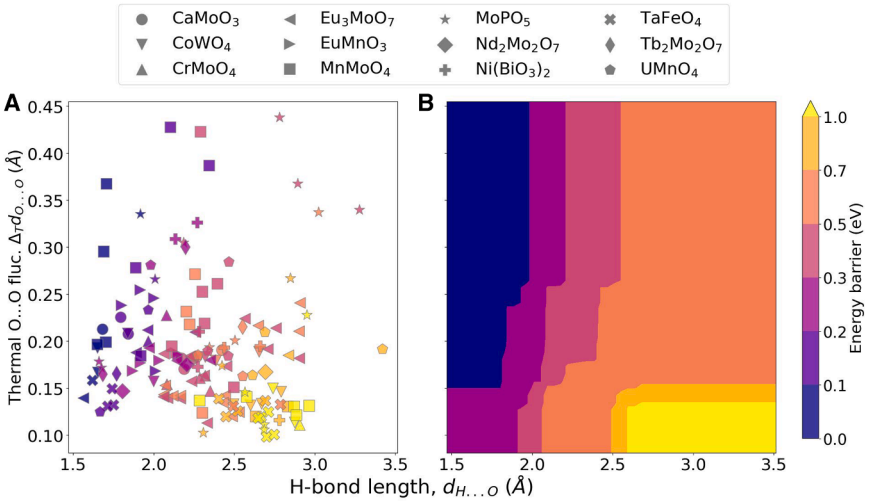


**Figure 8. Modeling energy barrier as a function of H-bond length and thermal O…O fluctuation**

(A) Scatterplot of proton-transfer energy barrier $E_a$ against thermal O…O fluctuation and H-bond length, with a point for each O…O pair, shapes indicating material containing the O…O pair, and darker colors showing lower energy barriers.

(B) Heatmap of energy barrier predicted by HGBDT model as function of H-bond length and thermal O…O fluctuation, using same color scale for $E_a$.

of performance must include all data points, this demonstrates that predictions were sufficiently accurate for most of the tested materials. A possible explanation for the outlier could be the out-of-distribution chemistry, as neither Sr nor Nb were present in our training data.

Quantitative accuracy of our regression model is uncertain for materials that differ significantly in chemistry or structure from those that were studied here. However, our results highlight the importance of these descriptors. In particular, our proposed dynamic descriptor, thermal O…O fluctuation, demonstrates predictive power and yields mechanistic insights. Given its promise, this could be a useful dynamic descriptor for other proton-conducting oxides, too, although the quantitative relations may change and can be explored in future works.

## O…O flexibility enables contraction during H-bond formation and proton transfer

By analyzing lattice distortions during H-bond formation and proton transfer, we further connect O-sublattice flexibility to underlying physical mechanisms and explain why thermal O…O fluctuation can strongly predict energy barrier. We first note that the transition state exhibited a characteristic O…O spacing of approximately 2.4 Å, as observed in case studies of doped and O-deficient $BaFeO_3$.[10,11] This constraint held across different chemical compositions and local structures in our data. At the transition state, the proton likely needs to be embedded into the valence shells of both the donor and acceptor,[15] and this requires the shrinking of the O…O spacing to the critical distance observed along the minimum-energy pathway.

To visualize changes in O…O spacings upon protonation, Figure 9A shows protonated spacing as a function of proton-free O…O spacing, with colors again indicating energy barriers. Points that fall farther below the $x = y$ line represent O…O pairs that

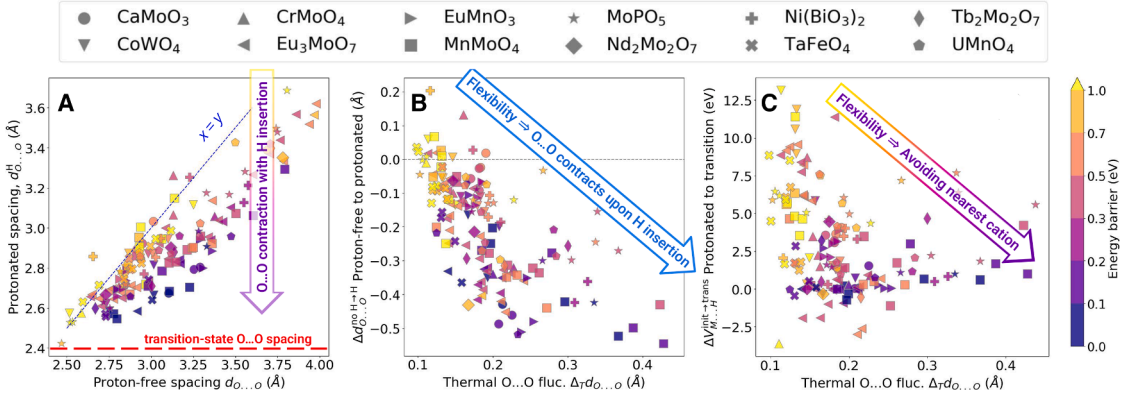


**Figure 9. Relations between O-sublattice flexibility and other descriptors**

(A) Protonated spacing plotted against proton-free spacing for all donor-acceptor pairs, with $x = y$ line corresponding to no contraction; effect of O…O contraction for fixed proton-free spacing illustrated by vertical arrow, with observed color gradient indicating lower energy barriers when O…O contraction is greater (shorter spacing when protonated).

(B) Change in proton-free to protonated O…O spacing plotted against thermal O…O fluctuation, with more flexible pairs undergoing larger decreases in spacing and being associated with lower energy barriers for proton transfer.

(C) Thermal O…O fluctuation ($x$-axis) vs. change in Coulombic repulsion between proton and nearest cation from initial to transition state, $\Delta V_{M\ldots H}^{init\rightarrow trans}$. Materials containing donor-acceptor pairs indicated by shapes. Energy barriers indicated by colors. Arrow with color gradient indicates observed trend of lower energy barriers with higher O…O flexibility and lower $\Delta V_{M\ldots H}^{init\rightarrow trans}$.

Please cite this article in press as: Chung et al., Flexibility of oxygen sublattice and hydrogen bond length predict proton mobility in ternary metal oxides, Matter (2025), https://doi.org/10.1016/j.matt.2025.102568



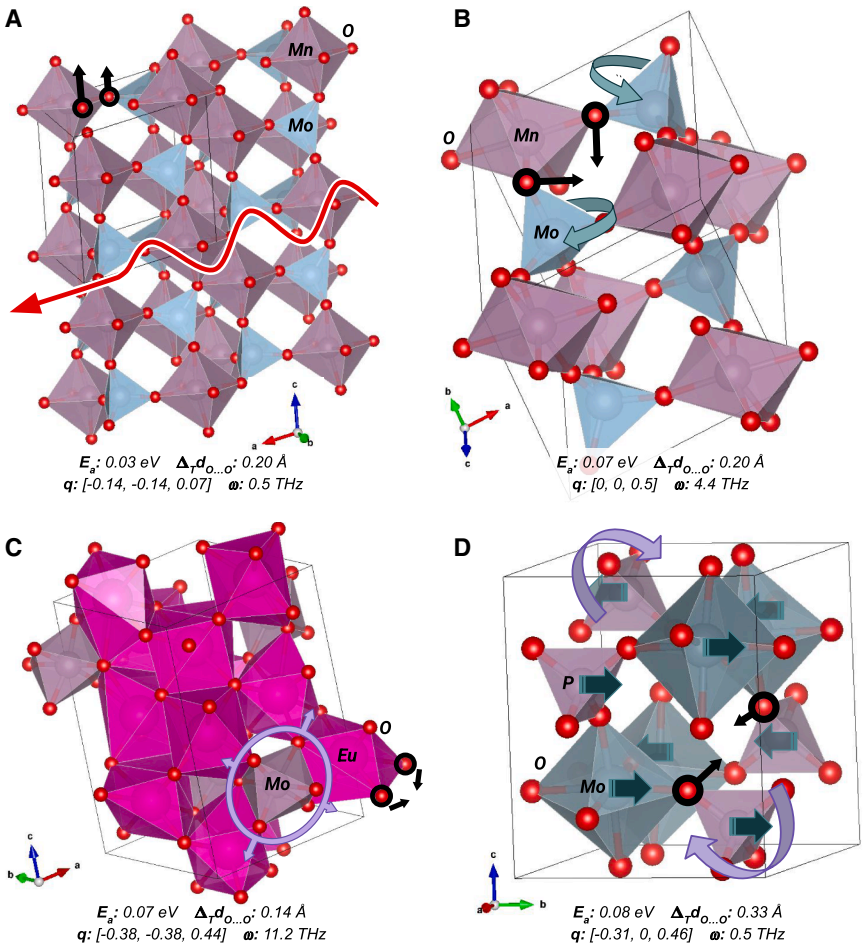


**Figure 10. Phonon modes dominating thermal O…O fluctuations for lowest-barrier O…O pairs**

Donor-acceptor pairs indicated with thick black outlines, where text below each mode lists calculated energy barrier, phonon wave vector, and phonon frequency.

(A) Red arrow representing transverse acoustic wave of oxide-ion displacements in $MnMoO_4$.

(B) O-Mn-O bending via $MoO_4$ tetrahedral tilt shown by blue arrows in $MnMoO_4$.

(C) O-Eu-O bending mode with $MoO_6$ octahedral breathing in $Eu_3MoO_7$.

(D) $PO_4$ tetrahedral tilt with shearing of (1 0 0) planes shown by purple and teal arrows in $MoPO_5$.

underwent greater contraction upon H insertion. For a fixed value of proton-free spacing, we observed a gradient toward lower barriers (dark purple) as protonated spacing decreases. This indicates that O…O pairs experiencing more contraction upon H insertion tended to subsequently enable more facile proton transfer. We can explain this trend by considering that all transition-state O…O spacings were close to 2.4 Å, visualized as a horizontal line in Figure 9A. Pairs farther below the $x = y$ line were closer to meeting the inherent constraint of this transition-state spacing and had to undergo less distortion along the proton-transfer pathway to meet 2.4 Å at the transition state. These same pairs, which showed more contraction upon protonation, also exhibited more flexibility, as demonstrated by the negative correlation between thermal O…O fluctuations and $\Delta d_{O...O}^{no\ H \to H}$ (Figure 9B). During subsequent proton-transfer, their compressions to ~2.4 Å would therefore incur lower energy costs, causing lower $E_a$.

## Oxygen-sublattice flexibility enables proton to reduce repulsion by cation during transfer

Tying one final property into our understanding of proton-transfer mechanisms, we explored the relation between dynamic and electrostatic descriptors. Figure 9C plots thermal O…O fluctuation against $\Delta V_{M...H}^{init \to trans}$, the change in Coulombic repulsion between the proton and its nearest cation from the initial to the transition state (Figure 2C). The negative correlation in Figure 9C suggests that more rigid donor-acceptor pairs forced protons to travel closer to the nearest cation during transport, whereas migration pathways across more flexible O…O pairs could better avoid these repulsions. Notably, pairs with higher flexibility and lower $\Delta V_{M...H}^{init \to trans}$ also tended to enable more facile proton transfer, evident from the color gradient indicated toward lower energy barriers.

## Phonon modes dominating thermal O…O fluctuations

Identifying the phonon modes that contribute most to thermal O…O fluctuations can be useful for finding strategies to maximize this physical descriptor and increase proton conductivity. We can extract these phonon modes from Equation 1 for visualization, as exemplified in Figure 10. Unlike other analyses that projected phonon modes onto ionic migration pathways,[21] our method of projecting the phonon modes onto the O…O axis isolates the effect of donor-acceptor flexibility from other lattice dynamics, which may affect proton transfer. Compared to projecting phonons onto the minimum-energy pathway, our method is less explicitly connected to energy barriers, but more directly estimating lattice flexibility. Since thermal O…O fluctuation can be calculated from the proton-free structure, this descriptor is also less computationally expensive and more appropriate for high-throughput screening. We summarize some trends we observed among modes dominating the thermal O…O fluctuations in our dataset.

Although there were no common phonons among those dominating thermal O…O fluctuations, we found that many tended to have low-frequency $\omega < 5$ THz (Figure 11A) and wave vectors at low-symmetry regions of the Brillouin zone (Figure 10). Some dominant modes (Figure 10D) for flexible lattices appeared to be combinations of higher-frequency with lower-frequency modes, similar to Mode B found for $BaZrO_3$ (Figure 3). We observed some negative correlation with thermal O…O

Please cite this article in press as: Chung et al., Flexibility of oxygen sublattice and hydrogen bond length predict proton mobility in ternary metal oxides, Matter (2025), https://doi.org/10.1016/j.matt.2025.102568





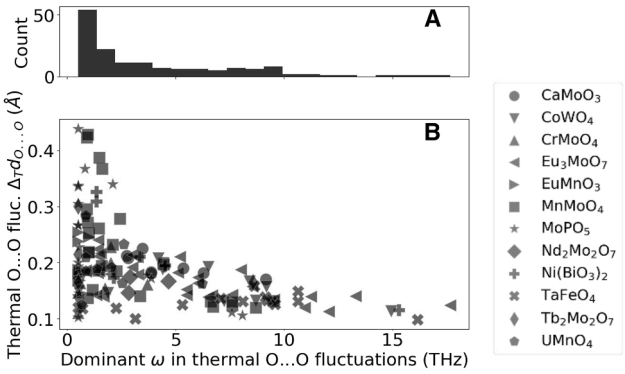


**Figure 11. Dominant frequencies of thermal O…O fluctuations**

(A) Distribution of frequencies for modes dominating thermal O…O fluctuation.

(B) Frequency of dominant phonon mode plotted against the overall thermal O…O fluctuation.

fluctuations (Figure 11B). This matched our expectation, since lower-frequency modes have higher phonon population and amplitude, making large thermal O…O fluctuations more likely.

## Conclusion

In this work, we introduced thermal O…O fluctuation as a dynamic descriptor that enabled direct comparison of O-sublattice flexibility across diverse oxides and offered new insight into physical mechanisms of proton conduction. Using a dataset of donor-acceptor pairs spanning varied local structures and chemistries, we systematically evaluated the predictive power of eight physically based descriptors, including our proposed measure of O-sublattice flexibility. Based on our modeling, the top two descriptors—H-bond length and thermal O…O fluctuations—captured as much information about proton-transfer energy barriers as the rest of the descriptors combined. Our bivariate model suggested that proton transfer is most facile across donor-acceptor pairs with H-bond lengths shorter than 2.0 Å and thermal O…O fluctuations greater than 0.15 Å at 600 K.

For O…O pairs with similar proton-free spacings, energy barriers tended to be lower for those that contract more and achieve a shorter spacing upon H-bond formation. More flexible donor-acceptor pairs contracted more upon H insertion and made more progress toward the characteristic transition-state spacing of 2.4 Å. This capacity for contraction was correlated with thermal O…O fluctuations, our measure of O-sublattice flexibility. Finally, we examined the phonon modes that dominated thermal O…O fluctuations and found that the frequency of the dominant mode decreased with increasing O-sublattice flexibility and those that contributed most to O…O fluctuations typically had frequencies below 5 THz.

Looking ahead, thermal O…O fluctuation is well suited for downstream high-throughput screening, since this descriptor is calculated from the proton-free configuration and requires no expensive calculations of structural relaxations to find stable protonated configurations or energy barriers of migration. In addition to this screening, optimizing proton conductivity will require insight into how our descriptors connect to tunable material properties. In particular, further work should investigate which properties can yield percolating paths of O…O pairs exhibiting high flexibility and strong H-bonding and how to construct such compounds. A generalized, quantitative understanding of phononic effects is also required for other factors contributing to proton conductivity, for example how lattice softness may accommodate protonic defects.[36] Though less common in ternary oxides, proton migration may be rate-limited by the hydroxyl bond rotation, requiring further exploration into how lattice dynamics may also affect this step and if there is a potential tradeoff between the resulting effects on proton transfer and hydroxyl rotation energies. Addressing these questions quantitatively will further enable materials discovery for hydrogen-based energy and computing devices.

## METHODS

For the case study of cubic $BaZrO_3$, phonon calculations were conducted under the harmonic approximation with Phonopy,[37] using a 3×3×3 supercell. Thermal O … O fluctuation was calculated for the nearest-neighbor O … O pair, setting the temperature to 600 K. Forces were obtained using the Perdew-Burke-Ernzerhof generalized gradient approximation functional with the Vienna Ab Initio Simulation Package.[38,39]

To collect our training and testing data, calculations were performed using the pretrained neural interatomic potential CHGNet[40] (Section S4). For training data, we started with materials proposed by Islam et al.[19] In their high-throughput screening, Islam et al. filtered over 5,000 ternary oxides from the Materials Project[32] based on water stability and hydrogen insertion energies. Since cation dopants to enable oxygen vacancies and hydration were not included in that work, only metal oxides containing multivalent cations could accommodate the electron accompanying the proton upon hydrogenation. Their final 28 candidates were, therefore, expected to be mixed electronic-ionic conductors. In particular, 19 of these materials contained Mo, Mn, or W, which are consequently common species in our training data. However, a variety of symmetries, energy barriers, and metal-oxygen $MO_x$ coordinations are still represented in this set (Table 2). This diverse dataset enabled us to evaluate the importance of thermal O…O fluctuations and other physical descriptors when predicting proton-transfer energy barriers. Although the materials considered are mixed ionic-electronic conductors, we only focus on proton-transfer mechanisms within these materials, leaving the electronic properties to future work.

For each of the candidate materials,[19] we computed the phonon band structure using the finite displacements method implemented in Phonopy[37] under the harmonic approximation. To screen for thermal stability, we removed structures with any predicted phonon frequencies below −1 THz and kept 12 of the remaining materials. Note that some materials in the test set, such as $BaZrO_3$, are known to require dopants to enable protonation. However, first-principles simulations have shown that the local charge distribution upon H insertion is independent of charge compensation.[12] Therefore, we only used undoped structures, simplifying phonon calculations and removing configurational complexity.

Within the 12 materials in the training set, we found 271 symmetrically unique O…O pairs, using a cutoff spacing of 4 Å. Without loss of generality, we assigned one oxide ion in each pair to be the donor and the other as the acceptor. In preparation for subsequent energy-barrier calculations, we found the initial protonated configuration by placing a proton 1 Å from the donor along the O…O axis, then performing structural relaxation with a convergence criterion of 0.05 eV/Å for maximal force. The final state was obtained in a similar manner, with the proton near the acceptor. For descriptor calculation, H-bond lengths and protonated O…O spacings were averaged over the initial and final states for each pair. Using this aggregation over the initial and final states, we therefore disregarded the direction of proton transfer.

We then performed climbing-image nudged-elastic-band (CI-NEB)[41] with nine images and convergence criterion of 0.05 eV/Å for maximal force. We retained only the pairs for which CI-NEB converged, so that our final dataset contained 153 pairs. For each O…O pair, we calculated all descriptors in Table 1 as inputs in our analysis, using the energy barrier of proton transfer as our labels. Energy barrier was defined as the difference between the highest and lowest energies along the minimum-energy pathway. Each thermal O…O fluctuation was calculated from the proton-free phonons integrated over the entire Brillouin zone, where temperature was set to 600 K and frequencies were clipped to a minimum of 0.5 THz. Supercells for all calculations were determined by ensuring that the shortest lattice vector was >20 Å.

Using the same interatomic potential and methods, we also constructed a test dataset. The constituent materials included perovskites, which had been previously studied for their proton-conducting properties.[12] There is structural variety in the test data, for example with the hexagonal $BaFeO_3$ containing face-sharing octahedra, as opposed to the cubic phase containing corner-sharing octahedra.

## RESOURCE AVAILABILITY

### Lead contact

Requests for further information and resources should be directed to and will be fulfilled by the lead contact, Bilge Yildiz (byildiz@mit.edu).

### Materials availability

This study did not generate new materials.

### Data and code availability

- All data reported in this paper will be shared by the lead contact upon request.
- This paper does not report original code.
- Any additional information required to reanalyze the data reported in this paper is available from the lead contact upon request.

## ACKNOWLEDGMENTS

This research is primarily supported as part of the Hydrogen in Energy and Information Sciences (HEISs), an Energy Frontier Research Center funded by the US Department of Energy (DOE), Office of Science, Basic Energy Sciences (BES), under award DE-SC0023450. H.W.C. also acknowledges support by the NSF Graduate Research Fellowship Program (GRFP), under award 2141064. High-performance computing resources were provided by the Texas Advanced Computing Center at The University of Texas at Austin under allocation DMR20012, as well as the National Energy Research Scientific Computing Center (NERSC), a DOE Office of Science User Facility using NERSC award BES-ERCAP-4584 for 2024 and BES-ERCAP-m4557 for 2025.

## AUTHOR CONTRIBUTIONS

Conceptualization, B.Y., J.L., H.W.C.; methodology, H.W.C. and P.Ž.; investigation, H.W.C.; writing–original draft, H.W.C.; writing–review & editing, B.Y., J.L., P.Ž., and H.W.C.; funding acquisition, B.Y., J.L., and H.W.C.; resources, B.Y. and J.L.; supervision, B.Y. and J.L.

## DECLARATION OF INTERESTS

The authors declare no competing interests.

## SUPPLEMENTAL INFORMATION

Supplemental information can be found online at https://doi.org/10.1016/j.isci.2024.110774.

Received: August 20, 2025
Revised: October 28, 2025
Accepted: November 11, 2025

## REFERENCES

1. Choi, S., Davenport, T.C., and Haile, S.M. (2019). Protonic ceramic electrochemical cells for hydrogen production and electricity generation: exceptional reversibility, stability, and demonstrated faradaic efficiency. Energy Environ. Sci. *12*, 206–215. https://doi.org/10.1039/C8EE02865F.
2. Liu, F., Deng, H., Diercks, D., Kumar, P., Jabbar, M.H.A., Gumeci, C., Furuya, Y., Dale, N., Oku, T., Usuda, M., et al. (2023). Lowering the operating temperature of protonic ceramic electrochemical cells to <450 °C. Nat. Energy *8*, 1145–1157. https://doi.org/10.1038/s41560-023-01350-4.
3. Schneller, T., and Schober, T. (2003). Chemical solution deposition prepared dense proton conducting Y-doped BaZrO3 thin films for SOFC and sensor devices. Solid State Ionics *164*, 131–136. https://doi.org/10.1016/S0167-2738(03)00308-4.
4. Onen, M., Emond, N., Wang, B., Zhang, D., Ross, F.M., Li, J., Yildiz, B., and del Alamo, J.A. (2022). Nanosecond protonic programmable resistors for analog deep learning. Science *377*, 539–543. https://doi.org/10.1126/science.abp8064.
5. Kreuer, K.D. (2003). Proton-Conducting Oxides. Annu. Rev. Mater. Res. *33*, 333–359. https://doi.org/10.1146/annurev.matsci.33.022802.091825.
6. Torayev, A., Sperrin, L., Gomez, M.A., Kattirtzi, J.A., Merlet, C., and Grey, C.P. (2020). Local Distortions and Dynamics in Hydrated Y-Doped BaZrO3. J. Phys. Chem. C *124*, 16689–16701. https://doi.org/10.1021/acs.jpcc.0c04594.
7. Regalado Vera, C.Y., Ding, H., Peterson, D., Gibbons, W.T., Zhou, M., and Ding, D. (2021). A mini-review on proton conduction of BaZrO3-based perovskite electrolytes. JPhys Energy *3*, 032019. https://doi.org/10.1088/2515-7655/ac12ab.
8. Zhang, W., and Hu, Y.H. (2021). Progress in proton-conducting oxides as electrolytes for low-temperature solid oxide fuel cells: From materials to devices. Energy Sci. Eng. *9*, 984–1011. https://doi.org/10.1002/ese3.886.
9. Lu, N., Zhang, Z., Wang, Y., Li, H.-B., Qiao, S., Zhao, B., He, Q., Lu, S., Li, C., Wu, Y., et al. (2022). Enhanced low-temperature proton conductivity in hydrogen-intercalated brownmillerite oxide. Nat. Energy *7*, 1208–1216. https://doi.org/10.1038/s41560-022-01166-8.
10. Hoedl, M.F., Chesnokov, A., Gryaznov, D., Merkle, R., Kotomin, E.A., and Maier, J. (2023). Proton migration barriers in BaFeO3−δ – insights from DFT calculations. J. Mater. Chem. A *11*, 6336–6348. https://doi.org/10.1039/D2TA08664F.

11. Chesnokov, A., Gryaznov, D., Kotomin, E.A., Maier, J., and Merkle, R. (2025). Protons in (Ga,Sc,In,Y)3+-doped BaFeO3 triple conductors — Site energies and migration barriers investigated by density functional theory calculations. Solid State Ionics *421*, 116788. https://doi.org/10.1016/j.ssi.2025.116788.

12. Bork, N., Bonanos, N., Rossmeisl, J., and Vegge, T. (2010). Simple descriptors for proton-conducting perovskites from density functional theory. Phys. Rev. B *82*, 014103. https://doi.org/10.1103/PhysRevB.82.014103.

13. Draber, F.M., Ader, C., Arnold, J.P., Eisele, S., Grieshammer, S., Yamaguchi, S., and Martin, M. (2020). Nanoscale percolation in doped BaZrO3 for high proton mobility. Nat. Mater. *19*, 338–346. https://doi.org/10.1038/s41563-019-0561-7.

14. Islam, M.S., Nolan, A.M., Wang, S., Bai, Q., and Mo, Y. (2020). A Computational Study of Fast Proton Diffusion in Brownmillerite Sr2Co2O5. Chem. Mater. *32*, 5028–5035. https://doi.org/10.1021/acs.chemmater.0c00544.

15. Kreuer, K.-D. (1996). Proton Conductivity: Materials and Applications. Chem. Mater. *8*, 610–641. https://doi.org/10.1021/cm950192a.

16. de Grotthuss, C.J.T. (1806). Sur la décomposition de l'eau et des corps qu'elle tient en dissolution à l'aide de l'électricité galvanique. Ann. Chim. *58*, 54–73.

17. Islam, M.S., Wang, S., Nolan, A.M., and Mo, Y. (2021). First-Principles Computational Design and Discovery of Novel Double-Perovskite Proton Conductors. Chem. Mater. *33*, 8278–8288. https://doi.org/10.1021/acs.chemmater.1c02432.

18. Kreuer, K. (2000). On the complexity of proton conduction phenomena. Solid State Ionics *136–137*, 149–160. https://doi.org/10.1016/S0167-2738(00)00301-5.

19. Islam, M.S., Wang, S., Hall, A.T., and Mo, Y. (2022). First-Principles Computational Design and Discovery of Solid-Oxide Proton Conductors. Chem. Mater. *34*, 5938–5948. https://doi.org/10.1021/acs.chemmater.2c00867.

20. Zhang, Z., Li, H., Kaup, K., Zhou, L., Roy, P.-N., and Nazar, L.F. (2020). Targeting Superionic Conductivity by Turning on Anion Rotation at Room Temperature in Fast Ion Conductors. Matter *2*, 1667–1684. https://doi.org/10.1016/j.matt.2020.04.027.

21. Gordiz, K., Muy, S., Zeier, W.G., Shao-Horn, Y., and Henry, A. (2021). Enhancement of ion diffusion by targeted phonon excitation. Cell Rep. Phys. Sci. *2*, 100431. https://doi.org/10.1016/j.xcrp.2021.100431.

22. Muy, S., Schlem, R., Shao-Horn, Y., and Zeier, W.G. (2021). Phonon–Ion Interactions: Designing Ion Mobility Based on Lattice Dynamics. Adv. Energy Mater. *11*, 2002787. https://doi.org/10.1002/aenm.202002787.

23. Li, X., and Benedek, N.A. (2015). Enhancement of Ionic Transport in Complex Oxides through Soft Lattice Modes and Epitaxial Strain. Chem. Mater. *27*, 2647–2652. https://doi.org/10.1021/acs.chemmater.5b00445.

24. Žguns, P., Klyukin, K., Wang, L.S., Xiong, G., Li, J., Haile, S.M., and Yildiz, B. (2024). Uncovering fast solid-acid proton conductors based on dynamics of polyanion groups and proton bonding strength. Energy Environ. Sci. *17*, 5730–5742. https://doi.org/10.1039/D4EE01219D.

25. Münch, W., Seifert, G., Kreuer, K.D., and Maier, J. (1997). A quantum molecular dynamics study of the cubic phase of BaTiO3 and BaZrO3. Solid State Ionics *97*, 39–44. https://doi.org/10.1016/S0167-2738(97)00085-4.

26. Kreuer, K.D., Münch, W., Traub, U., and Maier, J. (1998). On proton transport in perovskite-type oxides and plastic hydroxides. Ber. Bunsenges. Phys. Chem. *102*, 552–559. https://doi.org/10.1002/bbpc.19981020339.

27. Braun, A., and Chen, Q. (2017). Experimental neutron scattering evidence for proton polaron in hydrated metal oxide proton conductors. Nat. Commun. *8*, 15830. https://doi.org/10.1038/ncomms15830.

28. Du, P., Li, N., Ling, X., Fan, Z., Braun, A., Yang, W., Chen, Q., and Yelon, A. (2022). Optimizing the Proton Conductivity with the Isokinetic Temperature in Perovskite-Type Proton Conductors According to Meyer–Neldel Rule. Adv. Energy Mater. *12*, 2102939. https://doi.org/10.1002/aenm.202102939.

29. Wakamura, K. (2005). Empirical relationships for ion conduction based on vibration amplitude in perovskite-type proton and superionic conductors. J. Phys. Chem. Solid. *66*, 133–142. https://doi.org/10.1016/j.jpcs.2004.08.044.

30. Gomez, M.A., Griffin, M.A., Jindal, S., Rule, K.D., and Cooper, V.R. (2005). The effect of octahedral tilting on proton binding sites and transition states in pseudo-cubic perovskite oxides. J. Chem. Phys. *123*, 094703. https://doi.org/10.1063/1.2035099.

31. Dove, M.T. (1993). Introduction to Lattice Dynamics (Cambridge University Press). https://doi.org/10.1017/CBO9780511619885.

32. Jain, A., Ong, S.P., Hautier, G., Chen, W., Richards, W.D., Dacek, S., Cholia, S., Gunter, D., Skinner, D., Ceder, G., and Persson, K.A. (2013). Commentary: The Materials Project: A materials genome approach to accelerating materials innovation. APL Mater. *1*, 011002. https://doi.org/10.1063/1.4812323.

33. Ke, G., Meng, Q., Finley, T., Wang, T., Chen, W., Ma, W., Ye, Q., and Liu, T.-Y. (2017). LightGBM: A Highly Efficient Gradient Boosting Decision Tree. In Advances in Neural Information Processing Systems (Curran Associates, Inc.).

34. Ferri, F.J., Pudil, P., Hatef, M., and Kittler, J. (1994). Comparative study of techniques for large-scale feature selection. In Machine Intelligence and Pattern Recognition Pattern Recognition in Practice IV, E.S. Gelsema and L.S. Kanal, eds. (North-Holland), pp. 403–413. https://doi.org/10.1016/B978-0-444-81892-8.50040-7.

35. Steiner, T. (2002). The Hydrogen Bond in the Solid State. Angew. Chem. Int. Ed. *41*, 48–76. https://doi.org/10.1002/1521-3773(20020104)41:1%3C48::AID-ANIE48%3E3.0.CO;2-U.

36. Tsujikawa, K., Hyodo, J., Fujii, S., Takahashi, K., Tomita, Y., Shi, N., Murakami, Y., Kasamatsu, S., and Yamazaki, Y. (2025). Mitigating proton trapping in cubic perovskite oxides via ScO6 octahedral networks. Nat. Mater. https://doi.org/10.1038/s41563-025-02311-w.

37. Togo, A., Chaput, L., Tadano, T., and Tanaka, I. (2023). Implementation strategies in phonopy and phono3py. J. Phys. Condens. Matter *35*, 353001. https://doi.org/10.1088/1361-648X/acd831.

38. Perdew, J.P., Burke, K., and Ernzerhof, M. (1996). Generalized Gradient Approximation Made Simple. Phys. Rev. Lett. *77*, 3865–3868. https://doi.org/10.1103/PhysRevLett.77.3865.

39. Kresse, G., and Hafner, J. (1993). Ab initio molecular dynamics for liquid metals. Phys. Rev. B *47*, 558–561. https://doi.org/10.1103/PhysRevB.47.558.

40. Deng, B., Zhong, P., Jun, K., Riebesell, J., Han, K., Bartel, C.J., and Ceder, G. (2023). CHGNet as a pretrained universal neural network potential for charge-informed atomistic modelling. Nat. Mach. Intell. *5*, 1031–1041. https://doi.org/10.1038/s42256-023-00716-3.

41. Henkelman, G., Uberuaga, B.P., and Jónsson, H. (2000). A climbing image nudged elastic band method for finding saddle points and minimum energy paths. J. Chem. Phys. *113*, 9901–9904. https://doi.org/10.1063/1.1329672.